Hydrogen in $RE_6Fe_{13}XH_y$ intermetallic compounds (RE = Pr, Nd; X=Ag, Au, Si, Ge, Sn, Pb)

1996 J. Phys.: Condens. Matter 8 3453

(http://iopscience.iop.org/0953-8984/8/19/020)

J. Phys.: Condens. Matter **8** (1996) 3453–3469. Printed in the UK

Hydrogen in $RE_6Fe_{13}XH_y$ intermetallic compounds (RE = Pr, Nd; X = Ag, Au, Si, Ge, Sn, Pb)

A Leithe-Jasper†‡, R Skomski†, Qinian Qi†, J M D Coey†, F Weitzer‡ and P Rogl‡

† Department of Physics, Trinity College, Dublin 2, Ireland
‡ Institut für Physikalische Chemie der Universität Wien, Währingerstrasse 42, A-1090 Wien, Austria

Received 20 October 1995, in final form 7 February 1996

Abstract. The tetragonal ternary intermetallics $RE_6Fe_{13}X$(RE = Pr, Nd; X = Ag, Au, Si, Ge, Sn, Pb), which all crystallize in the $Nd_6Fe_{13}Si$ structure, are found to absorb approximately 12–18 hydrogen atoms/formula unit in a largely irreversible reaction at 390 K under a gas pressure of 1 bar. The unit cell volume expands by 10–15% without any change in the crystal symmetry and structure type, corresponding to an increase of volume per hydrogen atom of $\sim 2.9 \times 10^{-3}$ nm^3. Lattice expansion is highly anisotropic, being an order of magnitude greater along c than along a. The anisotropic lattice expansion and hydrogenation characteristics are explained in a model where the hydrogen atoms enter the ~ 0.7 nm rare-earth slabs in an amount controlled by the element X. The ~ 0.5 nm iron slabs expand little. Magnetization and Mössbauer measurements on the parent compounds show them to be essentially antiferromagnetic with a net moment of 0–1 μ_B/formula unit but on hydrogenation there is ferromagnetic behaviour with a moment of 23–27 μ_B/formula unit at room temperature.

1. Introduction

A search for new rare-earth iron alloys which may be useful as hard magnetic materials has continued over the past decade. Iron-based alloys are desirable for reasons of cost, and because iron has the largest magnetization of the 3d elements. However, dense-packed iron-based alloys are weak ferromagnets with a pronounced tendency towards antiferromagnetic interaction at small iron–iron distances. Hence they has been an interest in modifying their magnetic properties by inserting small atoms from the gas phase (hydrogen, nitrogen). All these issues are discussed in a new book [1]. Iron compounds of the $RE_6Fe_{13}X$ family are frequently obtained when transition-metal-rich alloys with X additives are prepared as starting materials for $RE_2Fe_{14}B$-type permanent magnets [2, 3]. It is of interest to understand the effect of hydrogen on their magnetic properties both as a problem in solid-state magnetism and also because hydrogen is increasingly used in the manufacture of rare-earth iron permanent magnets, and magnetic impurity phases may have a critical influence on coercivity [1].

A great many ternary intermetallics with general formula $RE_6T_{13-x}X_{1+x}$ (RE = light rare earth, T = Fe, Co; X = Cu, Ag, Au, Zn, Cd, Hg, Al, Ga, In, Tl, Si, Ge, Sn, Pb, As, Sb, Bi) [4–7], crystallize in the body centred tetragonal $Nd_6Fe_{13}Si$ structure type with $I4/mcm$ space group symmetry [5] (figure 1), which is an ordered variant of the $La_6Co_{11}Ga_3$ structure type [8]. In many cases there is a homogeneity range within the overall 6:14

0953-8984/96/193453+17$19.50

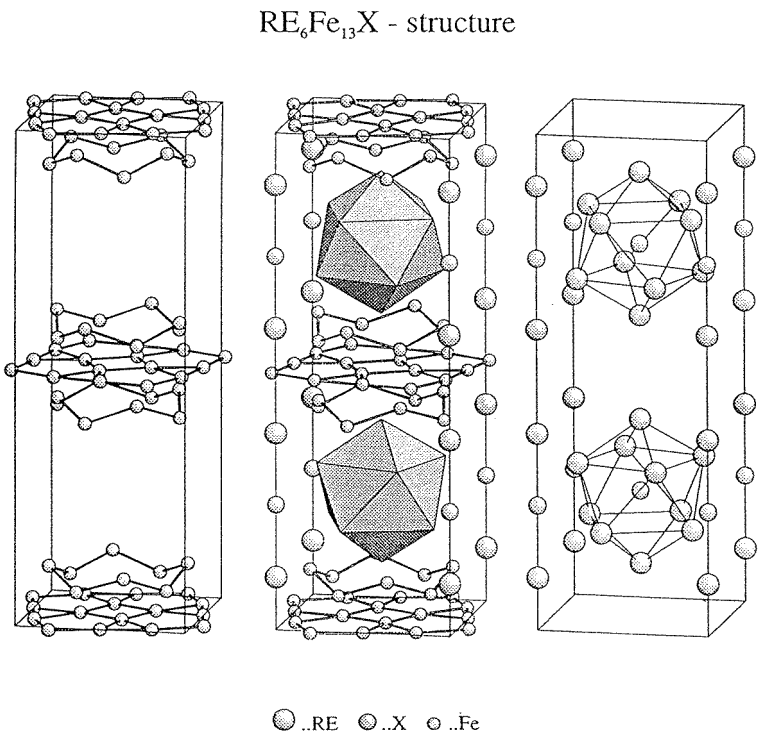

Figure 1. Crystal structure of $RE_6Fe_{13}X$.

stoichiometry. Precise atom parameters and interatomic distances have been derived from single-crystal x-ray counter data refinements of $Nd_6Fe_{13}Si$ [5], $Pr_6Fe_{13}Pb$ [6], $Nd_6Fe_{13}Au$ [7] and $Nd_6Fe_{13}Sb$ [9]. The crystallographic unit cell contains two rare-earth sites (16l, 8f), four iron sites ($16l_1$, 16k, $16l_2$, 4d) and one site (4a) which is occupied by X. The $RE_6Fe_{13}X$ crystal structure can be understood as a *multilayered* one where slabs of iron atoms alternate with slabs of rare-earth atoms (see figure 1). The iron slabs are built up of iron in $z = 0$ positions (16k, 4d) between puckered eight-membered rings of iron in $16l_1$ and $16l_2$ sites while the rare-earth slabs include a layer of X at the centre in the 4a site coordinated by a bicapped Archimedian antiprism [$R_{8+2}X$] of rare-earth atoms in 16l and 8f sites. All the atom positions derived for these compounds reveal a characteristic bonding scheme with Fe–Fe distances close to the sum of their atomic radii ($2r_{Fe} = 0.254$ nm). Only iron on the 4d site has a shorter average Fe–Fe distance (~ 0.24 nm) [6, 7, 9].

Several studies have been made of the magnetic properties of these compounds [2, 5, 6, 7, 9–14] which are relatively insensitive to the element X. Common features of the iron compounds are the following.

(i) They order magnetically near room temperature, in the range 250–550 K.

(ii) The net magnetization is considerably less than expected for collinear ferromagnetic alignment, being $\sim 1.5\ \mu_B\ fu^{-1}$ for 6:11:3 compounds [11, 15] and 0–2.0 $\mu_B\ fu^{-1}$ for 6:13:1 compounds [2, 4, 6, 11]. The small moments have been explained by ferrimagnetic [2, 6, 7, 11] or antiferromagnetic [12] spin arrangements.

(iii) Magnetic structures are at present unknown, but they are certainly complex. For example $Nd_6Fe_{13}Cu$ shows *c*-axis anisotropy, but none of the four iron sublattices has a

moment aligned along *c* [2].

(iv) Strong anisotropy exists for rare earths with $L \neq 0$. The electric field gradient is possibly of different sign at the two rare-earth sites [15].

(v) A sharp increase in slope of the magnetization curve is found in an applied field of 1–35 T [2, 11, 15–17]. Hysteresis is observed at the first-order magnetization process.

By contrast, the $La_6Co_{13}X$ compounds are ferromagnets with Curie temperatures ranging from 150 to 500 K, according to the nature of X. They seem to have canted ferromagnetic spin structures with a net moment of 12 μ_B fu^{-1} [6].

Here we analyse the influence of hydrogen on the crystal structure and magnetic properties of the iron-based intermetallics. We have already reported that the 6:13:1 compounds absorb prodigious quantities of hydrogen in an irreversible manner, and that the magnetization increases dramatically, to more than 30 μ_B fu^{-1}, without, however, attaining the value expected for collinear ferromagnetic alignment of all the rare-earth and iron sublattices [2, 9]. Here we describe the hydrogen uptake in more detail, and extend the chemical systematics with element X. The remarkable anisotropic hydrogen-induced strain and the main features of the magnetic behaviour are modelled by treating the 6:13:1 structure as an RE–Fe *multilayer* composed of alternating ~ 0.7 nm slabs of rare earth (and X) and ~ 0.5 nm slabs of iron, as seen in figure 1.

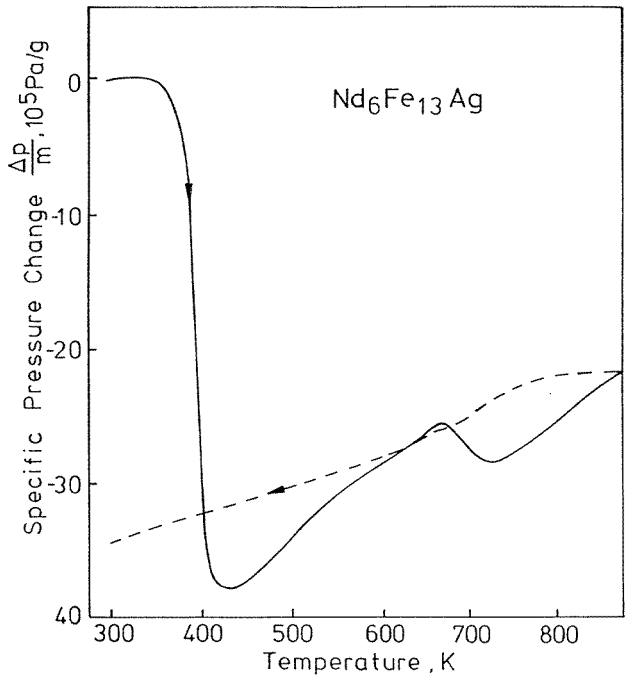

Figure 2. Typical hydrogen uptake for $Nd_6Fe_{13}Ag$ heated in hydrogen at a rate of 10 K min^{-1}.

2. Experimental methods

The ternary compounds with RE = Pr or Nd and X = Ag, Au, Si, Ge, Sn or Pb were prepared by arc melting pure elements (> 99.9%), followed by annealing at 870 K for

periods typically of 350 h. Details are given elsewhere [4, 6, 7]. X-ray powder diffraction was carried out at room temperature on all twelve parent compounds and the hydrogenated products.

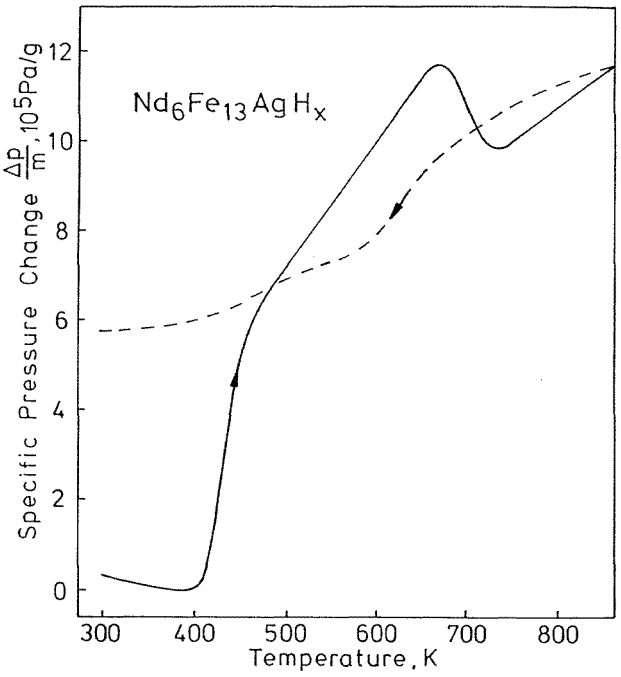

Figure 3. Degassing characteristics for $Nd_6Fe_{13}AgH_{18}$ heated in vacuum at a rate of 10 K min^{-1}.

Hydrogenation was carried out in a thermopiezic analyser (TPA) [18] where the sample is heated at a constant rate (10 K min^{-1}) in a small quartz tube connected to a fixed volume containing hydrogen gas, monitoring the pressure. The amount of the hydrogen absorbed was determined from the pressure drop observed in the TPA after cycling back to room temperature.

Magnetization curves were measured using a vibrating-sample magnetometer based on a novel permanent magnet configuration producing fields up to 1.1 T at room temperature [19].

Mössbauer spectra at 290 and 15 K were obtained using a conventional constant-acceleration spectrometer with a source of ^{57}Co in rhodium. The 15 K data were obtained using a closed-cycle two-stage helium refrigerator.

3. Results

3.1. Hydrogen uptake of $RE_6Fe_{13}X$ compounds

A typical hydrogen absorption curve is shown in figure 2 where the specific pressure change $\Delta P/m$ is plotted versus temperature. The two-stage reaction is typical of iron-rich rare-earth intermetallics such as Nd_2Fe_{17} [20], Sm_2Fe_{17} [20, 21] or $Nd_2Fe_{14}B$ [22]. A large quantity of hydrogen is taken up at about 390 K, and some of it leaks out again on further heating up to the onset of decomposition of the sample at approximately 670 K. The hydrogen content in

$R_6Fe_{13}X$ compounds cooled to room temperature in 1 bar hydrogen pressure ranges from 12 to 20 atoms per formula unit depending on the element X. The temperature for H absorption onset is slightly lower for the Pr-containing compounds than for the Nd-containing ones. Heating $Nd_6Fe_{13}AgH_{18}$ from vacuum in the TPA shows hydrogen loss beginning at 400 K (see figure 3). After heating to 870 K for 2 h in vacuum $Nd_6Fe_{13}AgH_{18}$ had decomposed into $NdH_{2+\delta}$, Fe, Ag and H_2. In order to obtain a further idea of the temperature stability of the $RE_6Fe_{13}XH_y$ compounds, the $Nd_6Fe_{13}AgH_{18}$ sample was annealed at temperatures from 400 K to 770 K under H_2. After heat treatment at 400, 420 and 570 K, samples revealed the $Nd_6Fe_{13}AgH_{18}$ structure whilst samples at 670 and 770 K showed complete decomposition into $NdH_{2+\delta}$, Fe and Ag (see table 2). Similar decomposition behaviour at 870 K was also observed for the compounds $Pr_6Fe_{13}AuH_{16.6}$ and $Pr_6Fe_{13}AuH_{13.6}$.

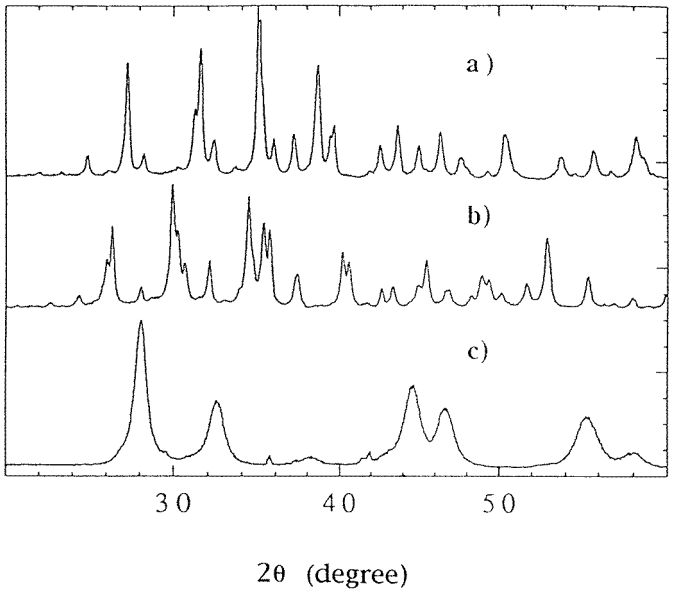

Figure 4. XRD patterns for (a) $Nd_6Fe_{13}Ag$, (b) $Nd_6Fe_{13}AgH_{18}$ hydrogenated at 420 K and (c) decomposed $Nd_6Fe_{13}AgH_{18}$ heated in H_2 at 670 K.

The powder XRD patterns of $Nd_6Fe_{13}Ag$, $Nd_6Fe_{13}AgH_{18}$, and the decomposition products are shown in figure 4. The hydrogen-loaded compound retains the same tetragonal structure as the parent compound with increased lattice parameters, especially in the *c* direction. The unit cell expands by 10–15% on hydrogen absorption, with an excess volume per absorbed hydrogen of 2.8–3.0 $\times 10^{-3}$ nm^3 for RE_6Fe_{13}(Si, Ge, Sn, Pb, Sb, Bi, Cu)H_x which is in agreement with the value of 2.9×10^{-3} nm^3 usually observed for intermetallic compounds [23]. RE_6Fe_{13}(Ag, Au)H_x show slightly enlarged excess volumes up to 3.4×10^{-3} nm^3 per hydrogen atom. The expansion of the *c* axis is in the range of 8–13%, whereas the expansion of the *a* axis is less than 2%. Lattice parameters and cell volume are summarized in table 1. The largest hydrogen uptake and lattice expansion are found when X = Cu, Ag and Au (see table 1 and figure 6), whereas the smallest effects are found for X = Sb, Sn, Bi and Pb.

Table 1. Crystallographic data for ternary alloys $RE_6Fe_{13}X$ and $RE_6Fe_{13}XH_y$ (RE = Pr, Nd; X = Ag, Au, Si, Ge, Sn and Pb), space group $I4/mcm$, $Nd_6Fe_{13}Si$ type.

Compound	a (nm)	$\Delta a/a$ (%)	c (nm)	$\Delta c/c$ (%)	V (nm^3)	$\Delta V/V$ (%)	c/a
$Pr_6Fe_{13}Ag$	0.8121(1)	—	2.2819(9)	—	1.5050(7)	—	2.810
$Pr_6Fe_{13}AgH_{17.0}$	0.8270(3)	1.7	2.5578(7)	12.1	1.7494(11)	16.2	3.092
$Pr_6Fe_{13}Au$	0.8098(1)	—	2.2659(6)	—	1.4860(6)	—	2.798
$Pr_6Fe_{13}AuH_{16.6}$	0.8204(2)	1.3	2.5474(7)	12.4	1.7145(9)	15.4	3.105
$Pr_6Fe_{13}Si$	0.8059(1)	—	2.2854(9)	—	1.4846(8)	—	2.835
$Pr_6Fe_{13}SiH_{14.7}$	0.8123(1)	0.7	2.5410(8)	11.2	1.6768(7)	12.9	3.128
$Pr_6Fe_{13}Ge$	0.8064(2)	—	2.2933(8)	—	1.4914(9)	—	2.843
$Pr_6Fe_{13}GeH_{13.9}$	0.8128(1)	0.8	2.5421(8)	10.8	1.6798(8)	12.6	3.127
$Pr_6Fe_{13}Sn$	0.8097(2)	—	2.3499(9)	—	1.5407(10)	—	2.902
$Pr_6Fe_{13}SnH_{13.6}$	0.8189(4)	1.1	2.5425(9)	8.2	1.7053(10)	10.7	3.104
$Pr_6Fe_{13}Pb$	0.8118(2)	—	2.3574(9)	—	1.5539(7)	—	2.903
$Pr_6Fe_{13}PbH_{13.1}$	0.8199(1)	1.0	2.5425(7)	7.9	1.7092(7)	10.0	3.101
$Nd_6Fe_{13}Ag$	0.8104(2)	—	2.2715(9)	—	1.4920(9)	—	2.802
$Nd_6Fe_{13}AgH_{18.0}$	0.8230(1)	1.5	2.5438(7)	12.0	1.7230(9)	15.5	3.091
$Nd_6Fe_{13}Au$	0.8090(2)	—	2.2602(6)	—	1.4793(4)	—	2.793
$Nd_6Fe_{13}AuH_{16.6}$	0.8190(1)	1.2	2.5316(6)	12.0	1.6981(7)	14.8	3.091
$Nd_6Fe_{13}Si$	0.8040(1)	—	2.2771(7)	—	1.4720(6)	—	2.832
$Nd_6Fe_{13}SiH_{14.7}$	0.8103(2)	0.8	2.5254(8)	10.9	1.6581(10)	12.6	3.116
$Nd_6Fe_{13}Ge$	0.8046(1)	—	2.2836(8)	—	1.4784(7)	—	2.838
$Nd_6Fe_{13}GeH_{14.5}$	0.8098(2)	0.6	2.5266(7)	10.6	1.6570(11)	12.1	3.119
$Nd_6Fe_{13}Sn$	0.8089(1)	—	2.3354(9)	—	1.5282(7)	—	2.887
$Nd_6Fe_{13}SnH_{13.3}$	0.8163(3)	0.9	2.5245(9)	8.1	1.6822(10)	10.1	3.092
$Nd_6Fe_{13}Pb$	0.8088(1)	—	2.3417(9)	—	1.5318(8)	—	2.895
$Nd_6Fe_{13}PbH_{13.1}$	0.8164(1)	0.9	2.5267(6)	7.9	1.6844(7)	10.0	3.094

Table 2. Crystallographic data for $Nd_6Fe_{13}AgH_{18}$ and $Pr_6Fe_{13}AuH_{16.6}$ annealed in hydrogen atmosphere at different temperature for 1–3 h.

Experimental conditions	Phase analysis	Lattice parameters (nm)		
		a	c	V (nm^{-3})
398 K, H_2, 1 h	$Nd_6Fe_{13}AgH_{18}$	0.8230(1)	2.5438(7)	1.7230(1)
420 K, H_2, 3 h	$Nd_6Fe_{13}AgH_{18}$	0.8251(1)	2.5432(7)	1.7317(1)
570 K, H_2, 3 h	$Nd_6Fe_{13}AgH_{18}$	0.8232(1)	2.5425(8)	1.7232(2)
770 K, H_2, 3 h	NdH_{2+x}	0.5509(3)	—	0.1672(1)
	α-Fe	0.2861(2)	—	0.0234(4)
	Ag	0.4085(5)	—	0.0682(2)
870 K, H_2, 1 h	PrH_{2+x}	0.5560(3)	—	0.1719(2)
	α-Fe	0.2866(1)	—	0.0235(1)
	Au	traces		

3.2. Magnetization

Some typical magnetization curves (collected at room temperature) on fixed powder samples of $Nd_6Fe_{13}Sn$, $Nd_6Fe_{13}Au$, $Nd_6Fe_{13}SnH_{13.3}$ and $Nd_6Fe_{13}AuH_{16.6}$ are shown in figure 5. Before hydrogenation the curve shows either a small net magnetization ($Nd_6Fe_{13}Sn$) or no net magnetization ($Nd_6Fe_{13}Au$), but the magnetization of the hydrides is completely different. There ferromagnetic-like magnetization curves approach saturation at 1.1 T at

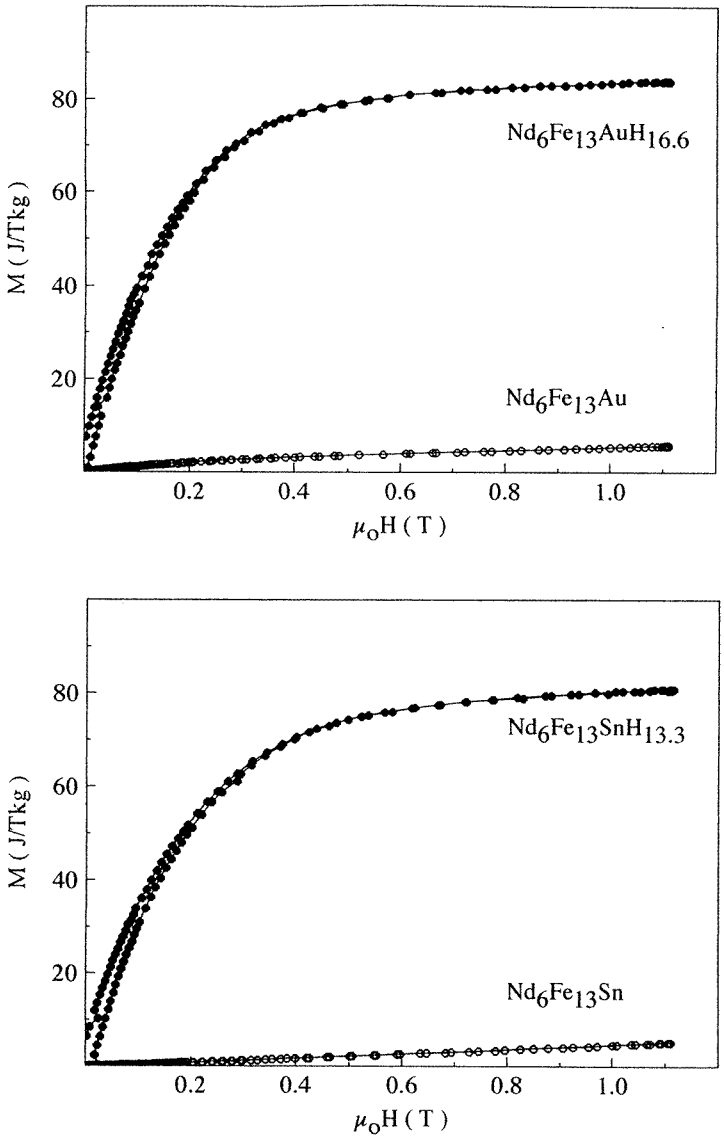

Figure 5. Magnetization curves for $Nd_6Fe_{13}Au$, $Nd_6Fe_{13}AgH_{16.6}$, $Nd_6Fe_{13}Sn$, $Nd_6Fe_{13}SnH_{13.3}$ measured at room temperature.

room temperature. The moment (table 3) is around 25 μ_B fu^{-1}.

3.3. Mössbauer spectroscopy

Some typical Mössbauer spectra of hydrogenated and parent compounds measured at 15 and 290 K are shown in figures 9–11. As for data on $RE_6Fe_{13}X(X = Sb, Bi)$ and their hydrogenation products reported previously [9] these spectra were fitted with four subspectra having an intensity ratio of approximately 1:4:4:4, which are associated with the four inequivalent iron sites 4d, 16k, $16l_1$ and $16l_2$. The subspectra are assigned on the basis

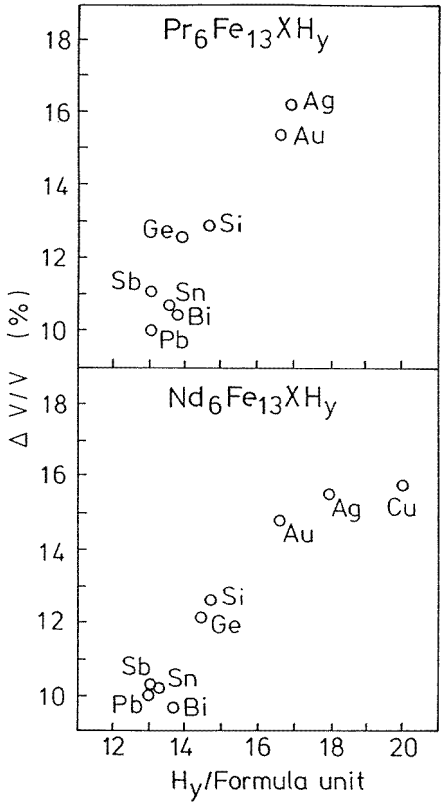

Figure 6. Volume expansion of $RE_6Fe_{13}XH_y$.

of intensity and the rule that iron neighbours tend to increase the ^{57}Fe hyperfine field and rare-earth nearest neighbours decrease it [24]. The largest hyperfine field is associated with the 4d sites which have 12 iron and no rare-earth neighbours. The smallest hyperfine field should be on $16l_2$ sites where there are seven iron and five rare-earth nearest neighbours. The 16k sites have 10 iron and two rare-earth neighbours whereas the $16l_1$ sites have nine iron and three rare-earth neighbours. Hence the order of hyperfine fields for different sites is $B_{hf}(4d) > B_{hf}(16k) > B_{hf}(16l_1) > B_{hf}(16l_2)$. Hyperfine fields are given in tables 3 and 4 and the average hyperfine fields are shown in figure 8.

4. Discussion

4.1. Hydrogenation and site occupancy

The two-stage reaction with hydrogen evident in figure 2 is typical of rare-earth intermetallics [20–22]. The two stages can be written schematically:

$$R_6Fe_{13}X + (y/2)H_2 \rightarrow R_6Fe_{13}XH_y \quad (1)$$

$$R_6Fe_{13}XH_y \rightarrow 6RH_{2+\delta} + 13Fe + X. \quad (2)$$

The decomposition products are more stable than hydrogen-loaded 6:13;1 intermetallics by an energy of the order of 600 kJ mol^{-1}.

Table 3. Magnetic properties of $RE_6Fe_{13}X$ and $RE_6Fe_{13}XH_y$ (RE = Pr, Nd; X = Si, Ge, Sn, Pb, Ag and Au).

	σ		$\langle B_{hf}\rangle$		$\langle \mu_{Fe}\rangle$	
	(JT^{-1} kg^{-1})	(μ_B fu^{-1})	(T)		(μ_B)	
Compound	293 K		15 K	293 K	15 K	293 K
$Pr_6Fe_{13}Ag$[a]	0.0	0.0	29.2	15.9	1.94	1.06
$Pr_6Fe_{13}AgH_{17.0}$	60.3	19.4	35.4	30.3	2.36	2.02
$Pr_6Fe_{13}Au$[a]	0.0	0.0	29.1	22.3	1.94	1.49
$Pr_6Fe_{13}AuH_{16.6}$	72.4	23.1	35.6	29.1	2.37	1.94
$Pr_6Fe_{13}Si$	0.0	0.0		22.3		1.49
$Pr_6Fe_{13}SiH_{14.7}$	78.1	22.6	30.6	23.9	2.04	1.59
$Pr_6Fe_{13}Ge$[b]	2.5	0.15	30.6	22.3	2.04	1.49
$Pr_6Fe_{13}GeH_{13.9}$	72.2	21.4	33.3	25.5	2.22	1.70
$Pr_6Fe_{13}Sn$	0.5	0.15		23.5		1.57
$Pr_6Fe_{13}SnH_{12.4}$	67.2	20.5	34.8	26.8	2.32	1.79
$Pr_6Fe_{13}Pb$	0.0	0.0		23.1		1.54
$Pr_6Fe_{13}PbH_{13.1}$	68.9	22.1	35.0	27.4	2.33	1.83
$Nd_6Fe_{13}Ag$[a]	0.0	0.0	29.5	23.7	1.97	1.58
$Nd_6Fe_{13}AgH_{18.0}$	61.0	18.8	36.2	30.7	2.41	2.05
$Nd_6Fe_{13}Au$[a]	0.0	0.0	29.4	22.7	1.96	1.51
$Nd_6Fe_{13}AuH_{16.6}$	76.9	24.9	35.2	28.3	2.35	1.89
$Nd_6Fe_{13}Si$	1.7	0.5		24.3		1.62
$Nd_6Fe_{13}SiH_{14.7}$	80.2	23.5	32.1	24.3	2.14	1.62
$Nd_6Fe_{13}Ge$[b]	3.0	0.7	30.0	24.3	2.0	1.62
$Nd_6Fe_{13}GeH_{14.5}$	75.9	22.8	32.2	23.8	2.15	1.59
$Nd_6Fe_{13}Sn$[c]	2.0	0.6	30.9	24.8		1.65
$Nd_6Fe_{13}SnH_{13.3}$	74.0	22.8	33.9	25.3	2.26	1.69
$Nd_6Fe_{13}Pb$[c]	0.6	0.2	30.8	24.9		1.66
$Nd_6Fe_{13}PbH_{13.1}$	70.4	22.6	34.8	25.3	2.32	1.69

[a] Mössbauer data at 4.2 K [4].
[b] Mössbauer data at 15 K [10].
[c] Mössbauer data at 4.2 K [3].

However, disproportionation is inhibited by the diffusion kinetics of the metal atoms. Gas-loaded iron-rich intermetallics normally decompose in the range 700–1000 K, whether they are hydrogen or nitrogen loaded [25]. This is the temperature where the diffusion length of iron reaches atomic dimensions on the experimental timescale. Since the diffusion constant of hydrogen is some 20 orders of magnitude greater than that of iron, it readily enters the intermetallic skeleton and forms the hydrogen-loaded intermetallic. The difficulty in removing all the hydrogen from $R_6Fe_{13}XH_y$ under vacuum (figure 3), unlike RE_2Fe_{17} or $R_2Fe_{14}B$, suggests that most of the absorbed hydrogen is firmly bound in the rare-earth slabs in the structure. The likely absorption sites are the interstices with rare-earth neighbours, which have been enumerated previously [9]. We note here the greater hydrogen absorption of 6:13:1 intermetallics with noble metals compared to metalloids, and the tendency for the absorption to decrease on passing down a column in the periodic table. Both tendencies may be rationalized by considering the enthalpies of reaction. At infinite dilution, the heat of reaction of hydrogen with Pr or Nd is about -50 and -60 kJ mol^{-1} [26], whereas with Ag or Si it is $+63$ and $+180$ kJ mol^{-1} [26], respectively.

The octahedral [$RE(1)_4RE(2)X$] 8f interstitial sites just above and below the $z = 1/4, 3/4$ planes (figure 1) have five RE and one X neighbours, whereas the 16l tetrahedral

Table 4. Mössbauer parameters of $RE_6Fe_{13}X$ and $RE_6Fe_{13}XH_y$ (RE = Pr, Nd; X = Ag, Au, Si, Ge, Sn, Pb, Sb, Bi).

	15 K				293 K			
Compounds	4d	16k	$16l_1$	$16l_2$	4d	16k	$16l_1$	$16l_2$
$Pr_6Fe_{13}Ag$[a]	36.3	32.2	30.0	23.5	26.1	23.8	17.8	3.7
$Pr_6Fe_{13}AgH_{17.0}$	39.3	37.4	34.6	33.1	32.8	32.5	29.7	28.0
$Pr_6Fe_{13}Au$[a]	36.6	32.8	30.1	23.5	27.3	24.1	23.9	17.6
$Pr_6Fe_{13}AuH_{16.6}$	38.6	36.9	34.1	34.9	31.9	30.5	29.1	26.9
$Pr_6Fe_{13}Si$					30.5	25.2	22.7	16.9
$Pr_6Fe_{13}SiH_{14.7}$	34.6	33.3	29.4	28.2	33.2	31.7	24.1	13.6
$Pr_6Fe_{13}Ge$[b]	34.9	34.2	30.7	25.8	29.9	25.3	22.7	17.0
$Pr_6Fe_{13}GeH_{13.9}$	35.2	34.9	32.6	31.9	27.9	26.8	26.6	22.6
$Pr_6Fe_{13}Sn$					30.1	28.3	23.8	16.5
$Pr_6Fe_{13}SnH_{12.4}$	37.9	35.9	35.5	32.3	29.6	28.0	27.5	24.1
$Pr_6Fe_{13}Pb$					28.2	28.2	23.2	11.8
$Pr_6Fe_{13}PbH_{13.1}$	38.1	35.6	34.9	33.8	29.4	28.6	28.4	24.7
$Nd_6Fe_{13}Ag$[a]	37.0	32.8	30.5	23.3	26.9	26.8	24.7	18.7
$Nd_6Fe_{13}AgH_{18.0}$	37.6	37.4	35.6	35.3	31.9	31.6	29.3	29.0
$Nd_6Fe_{13}Au$[a]	36.8	33.0	30.4	23.0	27.4	25.4	23.6	17.8
$Nd_6Fe_{13}AuH_{16.6}$	37.1	37.3	35.1	32.7	30.9	29.0	28.4	26.8
$Nd_6Fe_{13}Si$					28.3	27.7	25.6	18.7
$Nd_6Fe_{13}SiH_{14.7}$	34.3	32.7	32.8	30.3	27.6	25.6	25.1	21.4
$Nd_6Fe_{13}Ge$[b]	35.4	34.4	31.0	23.4	28.3	27.7	25.7	18.5
$Nd_6Fe_{13}GeH_{14.5}$	34.7	34.3	32.1	29.5	25.3	25.4	24.9	20.7
$Nd_6Fe_{13}Sn$[c]	36.5	34.5	33.3	23.7	29.3	28.4	26.3	18.6
$Nd_6Fe_{13}SnH_{13.3}$	36.9	35.0	34.9	31.1	28.2	27.2	26.0	22.1
$Nd_6Fe_{13}Pb$[c]	36.3	34.5	33.2	23.5	29.0	28.3	26.4	19.2
$Nd_6Fe_{13}PbH_{13.1}$	35.7	35.8	35.5	32.9	29.4	26.9	26.4	21.5

[a] Mössbauer data at 4.2 K [4].
[b] Mössbauer data at 15 K [10].
[c] Mössbauer data at 4.2 K [3].

$[RE(1)_4]$ interstices are entirely surrounded by RE atoms. The bond energies in these sites may be roughly estimated: for example the 8f octahedron has a bond energy $(5 \times (-50) + 63)/6 = -22.8$ kJ mol^{-1} when M = Ag but when M = Si the result is -3.3 kJ mol^{-1}, while the 16l $[RE(1)_4]$ tetrahedron seems to be the most stable configuration with bond energies of $(4 \times (-50))/4 = -50$ kJ mol^{-1}. The interstitial sites with one or two X neighbours are increasingly unfavourable as one goes down a column in the periodic table, since the occupancy becomes restricted due to the steric problem of increasing atomic size and the site bond energy becomes more positive.

In summary, the hydrogen is expected, from energetic considerations, to be bound in the rare-earth slabs, first in interstices with only RE neighbours, the 16l $[RE(1)_4]$ tetrahedra, next in the 16l $[RE(1)_3Fe(3)]$ and 16l $[RE(1)_2RE(2)Fe(3)]$ and 4c $[RE(2)_2Fe(2)_2]$ tetrahedra and finally in the sites with RE and X neighbours (two 8f $[RE(1)_5X]$ octahedral and 16l $[RE(1)_3X]$ tetrahedral sites). Occupancy of the latter sites strongly depends on the element X. No significant occupancy of the interstitials coordinated solely by iron can be expected. We obtain 84 interstices per unit cell summing up the previous mentioned sites. 52 of them have no X neighbours, being solely surrounded by (RE, Fe) atoms and occupation of them alone would account for 13 hydrogen atoms per formula unit as encountered in the RE_6Fe_{13}(Sn, Pb, Sb, Bi)H_{13} series. The environment of the remaining 32 sites (eight per

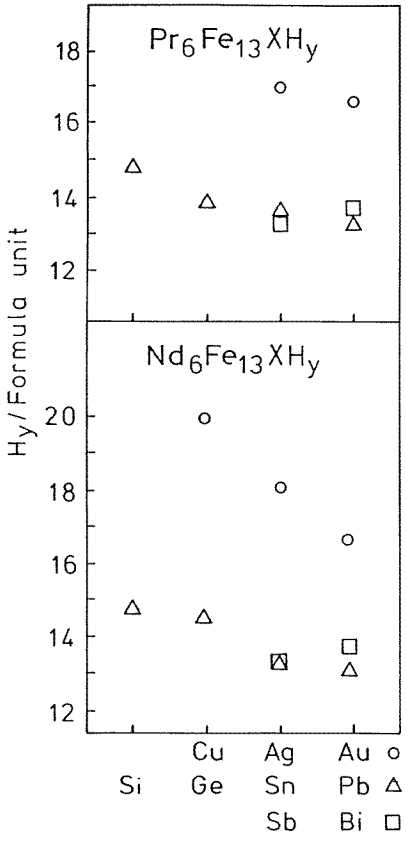

Figure 7. X-dependence of the hydrogen content in $RE_6Fe_{13}XH_y$ compounds.

formula unit) also contains X atoms and the higher H content of the other compounds (up to 20 atoms per formula unit observed in $Nd_6Fe_{13}CuH_{20}$) could be qualitatively described by successive filling of these sites with H atoms considering Westlake's rule, which forbids occupancy of interstitials which are closer than 0.21 nm [27].

4.2. Lattice expansion

Having seen that the hydrogen goes into the rare-earth slabs of the structure, giving them an approximate composition $RH_{2+\delta}$, while avoiding the iron layers, it is possible to understand the lattice expansion. The overall expansion per hydrogen atom has the familiar value of 2.9×10^{-3} nm^3 [23] but the remarkable feature of the 6:13:1 compounds is that the strain is highly *anisotropic*. We model this behaviour by considering a *multilayer* where Young's modulus and Poisson's ratio of the constituents are R_{RE} and ν_{RE} for the rare earth layer and E_{Fe} and ν_{Fe} for the iron layer respectively. To give a semiquantitative explanation for the much larger *c*-axis extension than *a*-axis extension (table 1) we make the following simplifying assumptions.

(i) The iron and rare-earth layers each obey Hooke's law for isotropic media:

$$\sigma_{ij} = \frac{E}{1+\nu}(\varepsilon_{ij} - \varepsilon_0\delta_j) + \frac{\nu E}{(1+\nu)(1-2\nu)}\delta_{ij}\mathrm{Tr}(\varepsilon_{ij} - \varepsilon_0\delta_{ij})$$

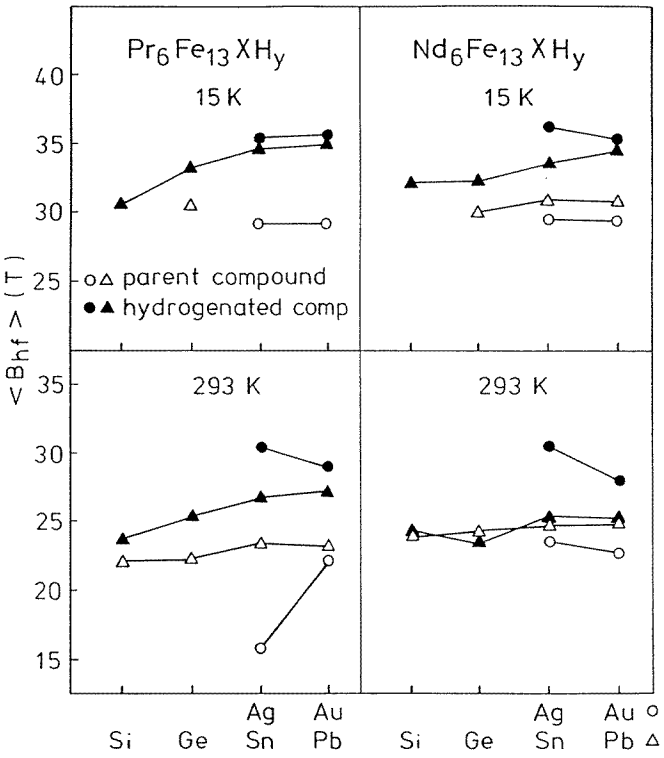

Figure 8. Variation of the average hyperfine field $\langle B_{hf} \rangle$ over all four inequivalent iron sites for $RE_6Fe_{13}XH_y$.

where E and ν are Young's modulus and Poisson's ratio, respectively. ε_0 is the linear lattice expansion of the unconstrained hydride; σ_{ij} and ε_{ij} are the stress and strain tensors, respectively.

(ii) The interstitial sites occupied by hydrogen are located in the rare-earth layers. Therefore $\varepsilon_0(\mathrm{RE}) = \varepsilon_{RE}$ and $\varepsilon_0(\mathrm{Fe}) = 0$.

(iii) Poisson's ratio is assumed to be the same for each layer, $\nu(\mathrm{RE}) = \nu(\mathrm{Fe}) = \nu$. Due to the tetragonal symmetry of the crystal, the principal components ε_{ii} of the strain tensor ε_{ij} obey $\varepsilon_{xx}(\mathrm{Fe}) = \varepsilon_{xx}(\mathrm{RE}) = \varepsilon_{yy}(\mathrm{Fe}) = \varepsilon_{yy}(\mathrm{RE}) = \varepsilon_{xx}$. The remaining three independent strain components ε_{xx}, $\varepsilon_{zz}(\mathrm{RE})$ and $\varepsilon_{zz}(\mathrm{Fe})$ are obtained by minimizing the elastic energy U_E:

$$U_E = \tfrac{1}{2} \sum_{ij=1}^{3} \int (\varepsilon_{ij} - \varepsilon_0 \delta_{ij}) \sigma_{ij} \, \mathrm{d}r.$$

The result [28] is

$$\varepsilon_{xx} = [f(\mathrm{RE}) E_{RE} / (f(\mathrm{RE}) E_{RE} + f(\mathrm{RE}) E_{Fe})] \varepsilon_R$$
$$e_{zz}(\mathrm{RE}) = [(1+\nu)/(1-\nu)] \varepsilon_{RE} - [2\nu/(1-\nu)] \varepsilon_{xx}$$

and

$$\varepsilon_{zz}(\mathrm{Fe}) = -[2\nu/(1-\nu)] \varepsilon_{xx}$$

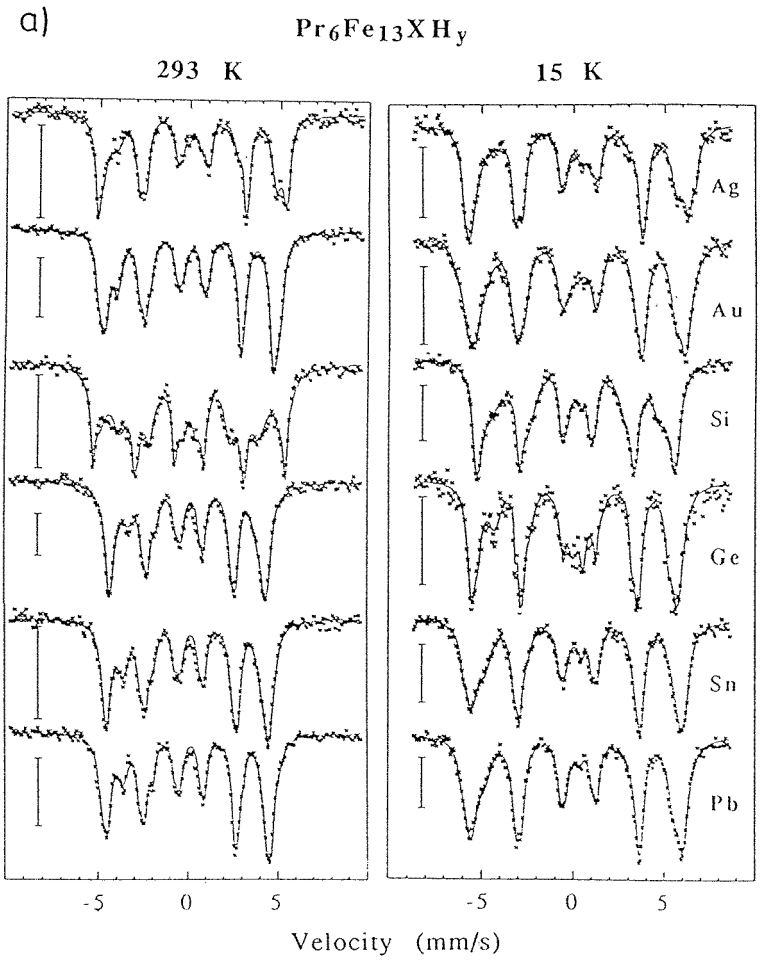

Figure 9. The ^{57}Fe Mössbauer spectra for (a) $Pr_6Fe_{13}XH_y$, (b) $Nd_6Fe_{13}XH_y$ at 293 K and 15 K and (c) $Pr_6Fe_{13}X$ and $Nd_6Fe_{13}X$ at 293 K (X = Ag, Au, Si, Ge, Sn and Pb). The fits described are shown by the full lines. Vertical bar represents 1% absorption.

where f denotes the volume fractions of the layers. Using $E_{Fe} = 215$ GPa and $E_{Fe} = E_{La} = 39$ GPa [29] and assuming $\nu = 1/3$, $\varepsilon_{RE} = 8\%$ and $f(\mathrm{RE}) = 0.6$, $f(\mathrm{Fe}) = 0.4$ we obtain $\varepsilon_{xx} = 1.7\%$, $\varepsilon_{zz}(\mathrm{Fe}) = -1.7\%$ and $\varepsilon_{zz}(\mathrm{RE}) = 14.3\%$. This implies $\Delta a/a = 1.7\%$ and $\Delta c/c = 7.9\%$, which is in fair agreement with the experimental values given in table 1. Closer accord is achieved by taking a smaller value of Young's modulus for the hydrogenated rare-earth layer, and a larger value for Poisson's ratio. For example if $E_{RE} = 20$ GPa and $\nu_{RE} = 0.4$, we find $\Delta a/a = 1.0\%$, $\Delta c/c = 10.0\%$. However, the assumption (i) of linear elasticity cannot be quantitatively accurate in view of the large strains involved.

4.3. The hyperfine field

There is evidence that the iron hyperfine field, particularly at the $16l_2$ sites, increases significantly after hydrogenation. The new field values are about 20% greater than in the

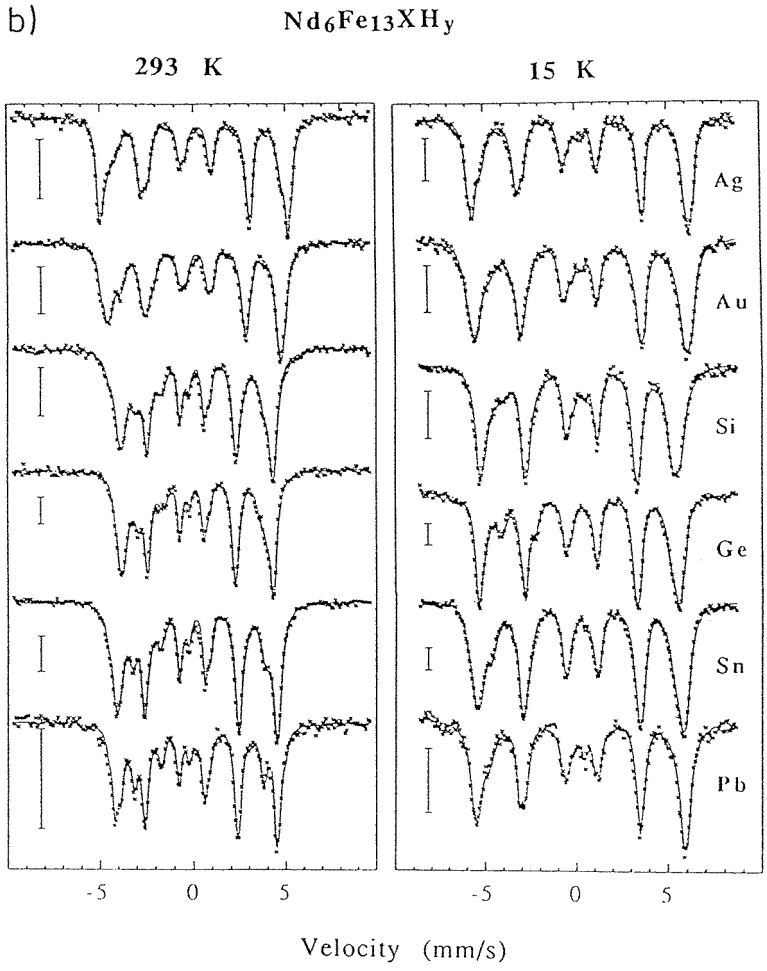

Figure 9. (Continued)

parent compounds and a similar increase of average iron moment is likely. Although the site moments in rare-earth intermetallics are not strictly proportional to their hyperfine fields, a fair correlation often exists between the average moment and the average hyperfine field [30]. The iron in related intermetallics is nearly a strong ferromagnet with a much greater density of states at the Fermi level in the $\downarrow$ subbands than in the $\uparrow$ subbands. The probable cause of the moment increase on hydrogenation is not so much volume expansion ($2\varepsilon_{xx}(\mathrm{Fe})+\varepsilon_{zz}(\mathrm{Fe})$ is unlikely to exceed 1–2% in the iron layers) as charge transfer towards the rare-earth–hydrogen units. The hydrogen in $REH_{2+\delta}$ is electronegative or anionic in character, which leaves the rare-earth atoms electron deficient. A charge transfer of ~ 0.3 electron/atom from the iron to the rare-earth atom could suffice to account for the increase of the iron moment. It is interesting that the effect of hydrogenation is greatest on the hyperfine fields of the $16l_2$ iron which has the largest number of rare-earth neighbours. Here there will be a direct effect when hydrogen occupies the 16l tetrahedral sites with three RE(1) and one Fe(3) neighbours.

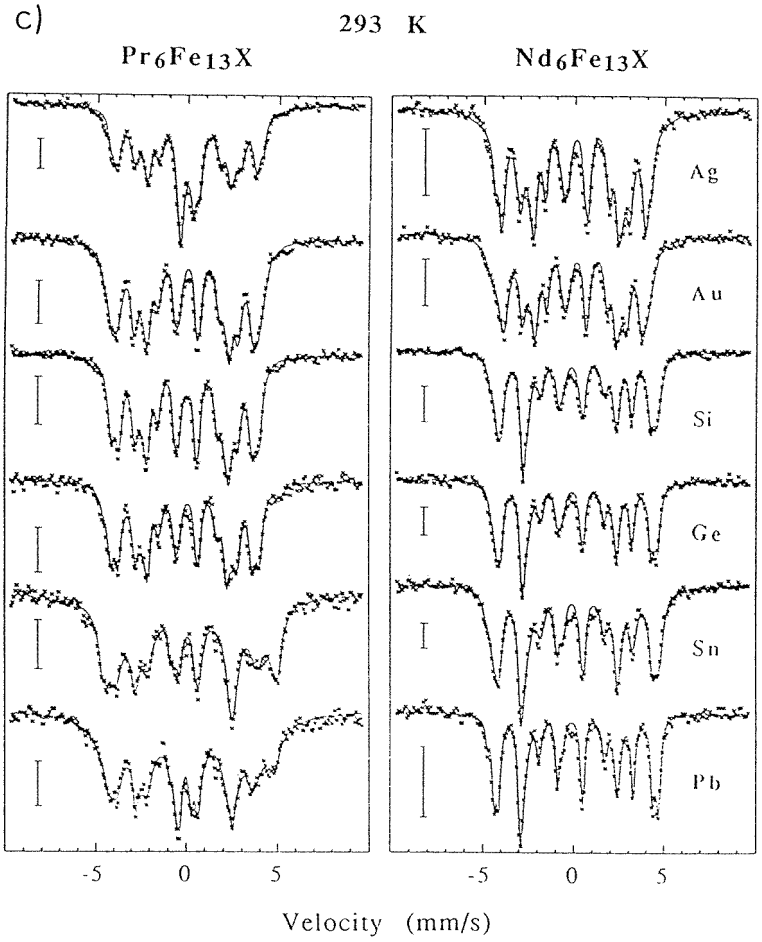

Figure 9. (Continued)

4.4. The isomer shift

The change in the isomer shift on hydrogenation ($\Delta IS = 0.15$ mm s^{-1}) is large. We have argued that the change in volume of the iron layer is only 1–2%, so the volume effect $\delta IS/\delta \ln V$ would only contribute 0.02 mm s^{-1} [31]. Most of the effect is due to a charge redistribution of iron electrons.

5. Discussion

It is interesting to compare the present results with those on hydrogen in RE–Fe and RE–Co binary alloys with a comparable ratio of 4d:3d elements. The data were reviewed by Wiesinger and Hilscher [32], The iron moment at low temperatures in $REFe_2$ ($MgCu_2$ structure) and $REFe_3$ ($PuNi_3$ structure) compounds is well established and is not much changed by hydrogen absorption. The net Fe–Fe exchange is weakened. In the cobalt alloys, the critical concentration for the appearance of magnetism lies close to the 1:2 composition. These alloys do not have a stable cobalt moment, and they exhibit band

metamagnetism [33]. However, the cobalt moment is well established in the 1:3 and 2:7 compounds. The first hydrogen absorbed in $RECo_3$ (β-phase) leads to a large, anisotropic expansion in the *c* direction [34], as in the present system. The preferred sites are likely to be in the vicinity of the rare-earth-rich planes in the $PuNi_3$ structure. However the effect of increasing hydrogen uptake is to reduce the magnetization, then increase it and then reduce it again, as the alloy changes from a ferromagnetic to an antiferromagnetic state. In contrast to $RE_6Fe_{13}X$ at high hydrogen loadings, which is driven from an antiferromagnetic to a ferromagnetic state, the effect of high hydrogen loading on the $RECo_3$ and RE_2Co_7 (γ-phases) is just the opposite [35], as the Co–Co intersublattice interaction becomes negative. The RE–Co interaction is significantly weakened on hydrogenation.

6. Conclusions

The large and partly irreversible hydrogen uptake in the 6:13:1 intermetallic compounds reflects the crystal structure which consists of alternating slabs of rare-earth atoms and iron atoms of thickness ~ 0.7 nm and ~ 0.5 nm respectively. The maximum hydrogen uptake is determined by the hydrogen disaffinity of the X atoms which lie at the heart of the RE slabs. Hydrogen is strongly bound in the tetrahedral interstices having only RE neighbours, but it is bound less strongly in the other interstitial sites in the RE slabs having one X neighbour or in the $[RE_3Fe]$ tetrahedral and $[RE_3Fe_3]$ octahedral sites. The hydrogenated intermetallics therefore combine characteristics of $RH_{2+\delta}$ hydrides and hydrogen solid solutions such as $RE_2Fe_{17}H_y$. The changes in the average iron hyperfine field and isomer shift indicate electron transfer away from the iron layers on hydrogenation. The disproportionation above 660 K is typical of hydrogen-loaded RE–Fe-intermetallics, which are metastable in a thermodynamic sense. They disproportionate into more stable products as soon as atomic diffusion permits.

Modelling the compounds as multilayers offers a semiquantitative explanation of the highly anisotropic lattice expansion in terms of the elastic properties of the two constituents. Although the details of the essentially antiferromagnetic structures of the parent compounds remain to be elucidated, hydrogen-induced metamagnetism is found in every case. The effect may perhaps be explained by a change in sign of the weak exchange coupling of the iron layers which is mediated by the rare-earth slabs. It is suggested that future work should be directed at the multilayer aspects of this family of compounds where nonmagnetic (La) or magnetic (Pr, Nd, Sm) rare-earth layers alternate with iron layers. The transport and magnetic properties of the lanthanum compounds in particular merit investigation.

Acknowledgments

This work was partly supported by the BRITE/EURAM programme of the European Committee. It forms part of the Concerted European Action on Magnets. Part of this research (ALJ and PR) has been sponsored by the Austrian Science Foundation (FWF projects S5605/4). PR wishes to acknowledge a grant from the Austrian National Bank (project no 3804). AL-J is grateful for support from the CEAM—Human Capital and Mobility programme for a research visit to Trinity College, Dublin.

References

[1] Coey J M D (ed) 1996 *Rare-earth Iron Permanent Magnets* (Oxford: Clarendon) p 512

[2] Knoch K G, Le Calvez A, Qi Q, Leithe-Jasper A and Coey J M D 1993 *J. Appl. Phys.* **73** 5878
[3] Knoch K G and Harris I R 1992 *Z. Metallk.* **83** 338
[4] Weitzer F, Klesnar H and Rogl P 1991 *Proc. Int. Conf. on Advanced Aluminium and Magnesium Alloys (Amsterdam, 1990)* ed T Kahn and G Effenberg (Metals Park, OH: ASM International) p 577
[5] Allemand J, Letant A, Moreau J M, Nozières J P, Perrier de la Bäthie R 1990 *J. Less-Common Met.* **166** 73
[6] Weitzer F, Leithe-Jasper A, Rogl P, Hiebl K, Noèl H, Wiesinger G and Steiner W 1993 *J. Solid State Chem.* **104** 368–76
[7] Weitzer F, Leithe-Jasper A, Rogl P, Hiebl K, Rainbacher A, Wiesinger G, Steiner W, Friedl J and Wagner F E 1994 *J. Appl. Phys.* **75**
[8] Sychevich O M, Lapunova P V, Sobolev A N and Grin Y 1985 *Crystallografiya* **30** 627
[9] Coey J M D, Qi Q, Knoch K G, Leithe-Jasper A and Rogl P 1994 *J. Magn. Magn. Mater.* **129** 87
[10] Grieb B, Henig E T, Martinek G, Stadelmaier H H and Petzow G 1990 *IEEE Trans. Magn.* **MAG-26** 1367
[11] Hu B P, Coey J M D, Klesnar H and Rogl P 1992 *J. Magn. Magn. Mater.* **177** 225
[12] Kajitani T, Nagayama K and Umeda T 1992 *Proc. 12th Int. Conf. on Rare Earth Magnets and their Applications (Canberra, 1992)* p 574
[13] Schrey P and Velicescu M 1991 *J. Magn. Magn. Mater.* **101** 417
[14] Rosenberg M, Zhou R J, Velicescu M, Schrey P and Filoti G 1993 *38th Ann. Conf. on Magnetism and Magnetic Materials (Minneapolis, MN, November 15–18, 1993)*
[15] Li H S, Hu B P, Cadogan J M, Coey J M D and Gavigan J P 1990 *J. Appl. Phys.* **67** 4841
[16] Zhao Z G, de Boer F R, Duijin V H M, Buschow K H J and Chuang Y C 1994 *J. Appl. Phys.* **75** 7117
[17] Zhao Z G, de Boer F R and Buschow K H J 1994 *8th Int. Symp. on Magnetic Anisotropy and Coercivity in RE–TM alloys (Birmingham, 1994)*
[18] Ryan D H and Coey J M D 1986 *J. Phys. E: Sci. Instrum.* **19** 693
[19] Cugat O, Byrne R, McCaulay J and Coey J M D 1994 *Rev. Sci. Instrum.* **65** 3570–3
[20] Wang X Z, Donnely K, Coey J M D, Chevalier B, Etourneau J and Berlureau T 1988 *J. Mater. Sci.* **23** 329
[21] Christodoulou C N and Takeshita T 1993 *J. Alloys Compounds* **113** 194
[22] Cadogan J M and Coey J M D 1986 *Appl. Phys. Lett.* **48** 442
[23] Peisl H 1978 *Hydrogen in Metals 1 (Topics in Applied Physics 28)* ed G Alefeld and J Völkl (Berlin: Springer) p 52
[24] Hu B P, Li H S and Coey J M D 1989 *Hyperfine Interac.* **45** 233
[25] Coey J M D 1996 *J. Magn. Magn. Mater.* at press
[26] Griessen R and Riesterer T 1988 *Hydrogen in Intermetallic Compounds I (Topics in Applied Physics 63)* ed L Schlapbach (Berlin: Springer) pp 266–9
[27] Westlake D G 1983 *J. Less-Common Met.* **90** 251
[28] Skomski R 1995 *Scripta Metall.* **33** 1831
[29] Ellis H 1984 *Book of Data* (Harlow: Longman)
[30] Qi Q, Sun H, Skomski R and Coey J M D 1992 *Phys. Rev.* B **42** 12 278–86
[31] Hu B P, Li H S, Sun H and Coey J M D 1991 *J. Phys.: Condens. Matter* **3** 3983–95
[32] Wiesinger G and Hilscher G 1991 *Ferromagnetic Materials* vol 6 ed K H J Buschow (Amsterdam: North-Holland)
[33] Levetin R Z and Markosyan A S 1988 *Sov. Phys.—Usp.* **31** 730
[34] Yamaguchi M, Ikeda H, Ohta T, Katayama T and Goto T 1985 *J. Less-Common Met.* **106** 165
[35] Bartashevich M I, Goto T, Yamaguchi M, Yamamoto I and Sugaya F 1993 *Physica* B **190** 319